Changes of the Arctic marginal ice zone

Rebecca J. Rolph, Daniel L. Feltham, David Schröder

Centre for Polar Observation and Modelling, Department of Meteorology, University of Reading, Reading, RG6 6BB, UK

Correspondence to: Rebecca J. Rolph (r.rolph@reading.ac.uk)

5   **Abstract.** Many studies have shown a decrease in Arctic sea ice extent. It does not logically follow, however, that the extent of the marginal ice zone (MIZ), here defined as the area of the ocean with ice concentrations from 15 to 80%, is also changing. Here, we present, for the first time, an analysis of satellite observations of pan-Arctic averaged MIZ extent. We find no trend in the MIZ extent during the last 40 years from observations. We present simulations from a coupled sea ice-ocean mixed layer model using a prognostic floe size distribution which we find is consistent with, but poorly constrained by, existing

10   satellite observations of pan-Arctic MIZ extent. We provide seasonal upper and lower bounds on MIZ extent based on the 4 satellite-derived sea ice concentration datasets used. An extrapolation of the observations shows the MIZ extent as remaining relatively constant in the coming decades, at least until the Arctic is completely covered by seasonal ice. We find a small increase in the summer MIZ fraction (MIZ extent divided by sea ice extent), which can be attributed to the reduction in total sea ice extent. The MIZ location is trending northwards, consistent with other studies. Given the results of this study, we

15   suggest that future studies need to remain cautious and provide a specific and clear definition when stating the MIZ is 'rapidly changing'.

1 Introduction

Arctic sea ice extent has been declining rapidly during the last 40 years (Comiso et al., 2008; Onarheim et al., 2018; Serreze et al., 2007; Stroeve et al., 2007). The MIZ has been variously defined as where ocean wind-generated waves interact with the

20   sea ice (e.g. Dumont et al., 2011) or as the area of ocean covered with 15-80% sea ice (e.g. Aksenov et al., 2017; Strong and Rigor, 2013). Due to its utility and the wealth of sea ice concentration data available, we use the latter operational definition of the MIZ extent being the total area of ocean capped by 15-80% sea ice cover. Given the rapid decline of sea ice extent in the Arctic, associated studies consequently tend to assume that the marginal ice zone (MIZ) extent is increasing (Boutin et al., 2019; Flocco et al., 2010; Horvat and Tziperman, 2015; Lee and Thomson, 2017; Strong et al., 2017; Tsamados et al., 2015).

25   The purpose of this paper is to show whether the extent of MIZ is actually changing. While there are significant regional changes happening in the Arctic MIZ such as increased light penetration (e.g. PAR), open water, and gas exchange (Barber et al., 2015), it is important to keep in mind that these changes are not necessarily a result of a change in the coverage of the total MIZ, but rather more likely the change in its location. As the Arctic MIZ moves northwards (Aksenov et al., 2017) the increased southward area of open ocean subsequently allows for increased wind-wave generation which can break up the ice

30   (Collins et al., 2015; Thomson and Rogers, 2014).   Thinner ice cover (Kwok, 2018) in combination with an increase in wind-wave action may result in smaller floes that melt faster due to an increased lateral melt rate (Tsamados et al., 2015).   The MIZ can also contribute to Arctic amplification because it is an area for Arctic cyclogenesis which is important for northward meridional heat transport (Inoue and Hori, 2011).   The MIZ supports many important processes such as Arctic marine primary production (Alexander and Niebauer, 1981), delivery of nutrients to the euphotic zone, air-sea gas exchange, and carbon
35   exchange across the air-sea interface (Barber et al., 2015; Hansen et al., 1996).   Monitoring changes of the MIZ environment in which these processes occur can help us understand the associated changes in the climate system.

It has been found that the width of the MIZ has increased in the summer and decreased in winter from 1979-2011 (Aksenov et al., 2017; Strong and Rigor, 2013).   However, it was also found that there is a positive (northward) trend in the area-weighted
40   latitude of the MIZ during the same time period (Strong and Rigor, 2013).   A northward trend of the MIZ and an increase of its (summer) width does not necessarily imply that the MIZ extent is increasing as the effective perimeter of the MIZ may be decreasing.   A decrease of total sea ice extent combined with a widening of the MIZ does imply, however, that the central pack ice will occupy less area.   This could ease Arctic access for ships (Aksenov et al., 2017). While the Arctic is projected to have entirely seasonal ice cover by mid-century (Notz and Stroeve, 2018; IPCC, 2014), a study of specific trends in MIZ extent is
45   lacking, such as quantification of the MIZ extent relative to the total sea ice extent.   Thus, we need to remain cautious and provide a specific and clear definition when stating the MIZ is 'rapidly changing'.   It also follows that we need to be aware of the extent to which our observations are able to constrain any model of the MIZ.   This paper aims to fill that gap.

We use a state-of-the-art sea ice-ocean model to better understand how well simulations can capture the satellite-observed
50   MIZ.   Due to the nature of the operational MIZ extent definition used here, this study can also be viewed as a test of model performance concerning how well sea ice concentrations are simulated on a pan-Arctic scale.   Winter, summer, and autumn months were selected to illuminate how well observations and simulation agree on a seasonal timescale. The bulk of the model set-up follows Schröder et al. (2019) and can be seen as representative of how well other models simulate sea ice concentration.

55   The paper set-up is as follows. In Section 2, we introduce the satellite observational datasets and model set-up we used. In Section 3, we describe the methods of applying our satellite data to our model grid, and subsequent analysis of the results. Here we also describe how we defined the MIZ and sea ice cover in our calculations. Section 4 presents our analysis of the extent of the total sea ice cover and MIZ as monthly averages for March, July, August, and September. It also includes trends and statistical analysis of the total MIZ extent relative to the total ice extent. Section 4 discusses the apparent change of location
60   in the MIZ. The subsequent discussion (Section 5) outlines possible implications of the trends we observe, and what this could mean for future projections of the MIZ.

2 Model set-up and Data

2.1 Observational datasets

The satellite products used in this study are: OSI-450 (EUMETSAT), NASA Bootstrap (Comiso, 2017), AMSR-E and AMSR-
65 2 (Spreen et al., 2008). OSI-450 is the second version of a processing of the EUMETSAT Ocean and Sea Ice Satellite
Application Facility (OSI SAF) team Sea-Ice Concentration (SIC) Climate Data Record (CDR). Sea ice concentration is
provided over the polar regions at 25 km resolution and derived from passive microwave satellite data SSMR, SSM/I and
SSMIS for years 1979 through 2015 (every other day from January 1, 1979 to August 20, 1987 and daily from August 21,
1987 through December 31, 2015). This processing includes using Numerical Weather Prediction re-analysis atmospheric
70 data to correct brightness temperature, dynamic tie-points, and state-of-the-art algorithms which are described in detail in
(Lavergne et al., 2016). The NASA Bootstrap sea ice concentration product has a 25 km resolution and is derived from
SSMR, SSM/I, and SSMIS sensors and generated using the AMSR-E Bootstrap Algorithm (Comiso, 2017) with daily data
available from November 1978 through 2018. The AMSR-E Bootstrap algorithm uses daily varying tie-points, three frequency
channels which are available continuously from SSMR, through SSM/I and to AMSR-E. All three of these channels have
75 vertical polarization and two of those have horizontal polarization. A basic assumption of the Bootstrap algorithm is that a
certain observational area is covered by entirely ice or water, which can lead to data smearing at the ice-ocean edge or in areas
where the contrast of emissivity between ice and water are not so strong. A higher resolution in general gives better chances
to distinguish the correct location of the ice edge and characterize the MIZ (Comiso, 2012).

80 AMSR-E v5 and AMSR-2 v5.4 are datasets processed using the ASI-algorithm (Spreen et al., 2008) and are the highest
resolution observational datasets used in this study with a grid spacing of 6.25 km. The time frame for available data for the
Japanese AMSR-E sensor onboard the EOS/Aqua satellite is from 1 June 2002 to 4 October 2011 and for the AMSR-2 sensor
onboard the GCOM-W satellite is from July 2012 to 17 November 2018. The ice concentration is calculated from the difference
of brightness temperatures in the vertical and horizontal polarization, which is a result of emissivity differences. At 90 GHz,
85 the emissivity of open water is much smaller than that of all ice types and so water can be distinguished from the ice. An
atmospheric correction is applied to account for the influence of the atmosphere on the upwelling polarization (Spreen et al.,
2008). This correction assumes a horizontally stratified Arctic atmosphere with an effective temperature to replace the vertical
temperature profile and a diffusely reflecting surface viewed under a 50º incidence angle (Svendsen et al., 1987). The ice
concentration then becomes a function of the polarization difference and the atmospheric correction term which is in general
90 also a function of ice concentration (Svendsen, 1983; Svendsen et al., 1987). Atmospheric influence is assumed to be a smooth
function of ice concentration and a third order polynomial for ice concentration is solved as a function of polarization
difference. Fixed tie points, which provide necessary values for unknowns, are found by comparing ice concentration from
the Svendsen algorithm and an ice concentration reference from an independent source that has been well validated (Spreen et
al., 2008). A weather filter is applied due to the disadvantage of the brightness temperatures from 89 GHz channels being

95 influenced by the atmospheric cloud liquid water and water vapor. Some sources of error include water vapor and wind roughening of the ocean influencing the polarization difference. Values for error between the different data products used in this study are given in Section 5.3.

2.2 Model set-up (CICE-CPOM-2019)

We use a dynamic-thermodynamic sea ice model, CICE-CPOM-2019, which is designed to be included in global climate
100 models. CICE-CPOM-2019 is based on the existing CICE model version 5.1.2, but with some additions. We perform a stand-alone (fully forced) simulation for the pan-Arctic region (~40 km grid resolution) with a spin-up of 10 years from 1979, and then restarted at 1979 and run through 2016. The CICE model solves 1-D vertical heat balance equations for 5 ice thickness categories. The momentum balance equation which provides the sea ice velocity includes air and ocean drag, the Coriolis force, sea surface tilt, and internal ice stresses. Hunke et al., (2015) gives a detailed description of the CICE model. Since we
105 did not use a coupled ocean model to calculate heat transport in the ocean or ocean currents, the temperature and salinity in the layer below the ocean mixed layer are restored every 20 days to climatological monthly means from MYO-WP4-PUM-GLOBAL-REANALYSIS-PHYS-001-004 (Ferry et al., 2011). Ocean currents are restored on the same timescale and from the same reanalysis dataset. For the atmospheric forcing, NCEP Reanalysis-2 (NCEP2) is used (Kanamitsu et al., 2002, updated 2017).

110

Some of the default CICE configurations used in this study include: seven vertical ice layers, one snow layer, thermodynamics of Bitz and Lipscomb (1999), Maykut and Untersteiner (1971) conductivity, the Rothrock (1975) ridging scheme with a Cf value of 12 (an empirical parameter that accounts for dissipation of frictional energy), the delta-Eddington radiation scheme (Briegleb and Light, 2007), and linear remapping ITD approximation (Lipscomb and Hunke, 2004). For CICE-CPOM-2019,
115 we switched on a prognostic melt pond model (Flocco et al., 2010, 2012), used an elastic anisotropic plastic rheology (Heorton et al., 2018; Tsamados et al., 2014; Wilchinsky and Feltham, 2006), a prognostic oceanic mixed layer (Petty et al., 2014) and a prognostic floe size distribution (Roach et al., 2018). Demonstrated use of CICE-CPOM-2019 including the above additions, with the exception of the prognostic mixed layer and floe size distribution, is provided as the reference simulation in Schröder et al. (2019). The prognostic mixed layer allows the ocean below the mixed layer to be relaxed toward observations so that
120 the mixed layer can calculate its salinity, temperature, and depth based on the fluxes from the deeper ocean (Petty et al., 2014). The prognostic floe size distribution is a new development (Roach et al., 2018) and warrants more detailed description which is provided in the next section.

2.2.1 Prognostic floe size distribution

A sea ice floe size distribution is a probability distribution function (Thorndike et al., 1975) that characterizes the extensive
125 variability (centimeters to hundreds of kilometers) in the range of sea ice floe sizes. Imposing a subgrid-scale floe size distribution (e.g. Bennetts et al., 2017; Zhang et al., 2016) does not account for physical processes acting on individual floes.

However, here we have added the recent development by Roach et al., (2018) into CICE-CPOM-2019, which accounts for ice formation, welding of floes, lateral freeze/melt, and fracture by ocean surface waves. Particularly important processes which determine the floe size evolution are lateral melt of floes and floes welding together, as well as wave fracture. When floes are

130 smaller, the lateral melt becomes more important, and this can lead to a significant reduction in sea ice concentration in summer (Roach et al., 2018). CICE simulates an ice thickness distribution and the sea ice concentration is calculated by integrating over all ice thickness categories. The change in the ice thickness distribution depends on growth/melt at a melting/freezing rate, ice advection, and redistribution of thickness categories caused by sea ice deformation. When the heat available from the surface of the ocean is enough to melt the ice, basal melting will occur by balancing the conductive heat flux from the bottom

135 and downward heat flux from the ice to the ocean. Lateral melt is obtained as a function of floe size. CICE uses a constant floe size of 300 m, but in CICE-CPOM-2019 a joint floe-size thickness distribution (FSTD) is used which has been developed by Roach et al. (2018) following the ice thickness distribution of Horvat and Tziperman, (2015).

The thermodynamic changes in the FSTD not included in the standard CICE model include a welding parameter for newly

140 formed floes to freeze together and a 'lead region' which is part of the open water fraction where lateral growth of existing floes can occur around non-circular floes. Mechanical breaking of sea ice floes by ocean surface waves is determined by a critical strain and minimum floe size (10 m) which can be impacted by wave fracture. The fractures that would occur if the waves enter an entirely ice-covered region defined in the 1-dimensional direction of propagation are calculated and then the outcome is applied proportionally to each grid cell's ice-covered fraction. Swell from hindcast wave data coming from the

145 equatorward meridional direction are used to select the significant wave height and mean period. This is then used to construct the wave spectrum (Bennetts et al., 2017; Horvat and Tziperman, 2015) which is attenuated exponentially given the number of floes in the grid cell, and is a function of ice thickness and wave period. With the assumption that sea ice flexes with the sea surface height field, the strain of the ice is calculated and the floe will fracture if this crosses a threshold. New floe radii are put into a histogram which depend on the local sea surface height field only.

3 Methods

3.1 Applying satellite-derived sea ice data to model grid

All available OSI-450, NASA Bootstrap, and AMSR data through 2017 (2015 for OSI-450) were interpolated onto the ORCA tripolar 1° grid. A tripolar grid allows a construct of a global orthogonal curvilinear ocean mesh that has no singularity point inside the computational domain because two north mesh poles are placed on land (Madec and Imbard, 1996). The ORCA

155 tripolar grid is used by CICE and so will hereafter be referred to as the 'CICE grid' for simplicity. We use about a 40 km resolution mesh, with the CICE land mask also applied. For NASA Bootstrap, AMSR-E, and AMSR2, a data gap at the pole exists in the downloaded product we filled in. To do this, after interpolating the daily satellite data to the CICE grid, we marked which grid cells at the pole were missing sea ice concentration data. Then, we re-gridded each daily file onto a lower-

resolution grid such that the missing values near the pole could no longer be resolved. We then applied this output back to the original higher resolution CICE grid. However, only the values of those grid cells which had previously been missing data on the CICE grid were kept from this method. One exception to this pole-filling method includes the years of 1979 through 1987 in the Bootstrap data, where the pole gap was larger than the rest of the Bootstrap data and the interpolation to the coarser grid still resolved some of the pole gap. Based on the high surrounding summer ice concentration (>80%) for these early years, the sea ice concentration within the pole gap is expected to be over 80%, so this was assumed for these years. The rest of the values in the CICE grid were taken via direct interpolation of the satellite data.

3.2 Calculating the marginal ice zone and sea ice extent

The MIZ extent was calculated as the total area of all grid cells between the thresholds of 15% and 80% sea ice cover, as the MIZ is also defined by other studies (e.g. Strong and Rigor (2013), Aksenov et al., (2017)). The daily values of MIZ extent were calculated for each of the observational datasets after they had been re-gridded to the model grid (and model land mask applied). The daily values of MIZ extent were also calculated for the model output. The daily total sea ice extent was also found for each dataset, which is defined as the total area of those grid cells which are covered by at least 15% sea ice. The daily MIZ extent was divided by the daily sea ice extent to get the daily relative MIZ extent. The monthly means of all these daily metrics were then calculated, and the main further analysis has used these monthly means. AMSR-E and AMSR-2 were combined into one time series, labelled AMSR, for the purpose of cross-correlating with the other datasets. We were unable to derive the error associated with these total measures of extent from the satellite products themselves due to uncertainties in the processing chains that prevent clear statements of error bounds. Following Spreen et al. (2008), we apply an error of 10%, based on systematic differences of monthly satellite products, to our calculated monthly means of the sea ice extent, MIZ extent, as well as the relative MIZ extent.

4 Results

4.1 Extent of marginal ice zone and total sea ice

The sea ice extent across the observational products do agree within their range of uncertainty. The model simulation agrees with the observations during winter, but slightly underestimates the summer ice extent (solid lines in Figure 1). The sea ice extent as calculated by the model still falls within the error range through July (solid lines in Figure 1b) and is underestimated starting in August (solid lines in Figure 1c) and September (solid lines in Figure 1d). However, by October, the ice extent is again within the 10% error range within the observational products. The March, July, August and September trends of declining total sea ice extent (Table 1) are significant with the exception of the modelled trend in the March sea ice extent. September shows the fastest rate of decline compared to the other months examined, consistent with other studies (Boé et al., 2009). There is also a significant high correlation between the inter-annual variability of sea ice extent observations for all months examined, with values greater than 0.957 in March and greater than 0.987 for July, August and September (Table 2).

190 The lowest correlations occur in March between the model and OSI-450 (0.448), the model and Bootstrap (0.587), and also in July between the model and AMSR (0.575).

In contrast with the sea ice extent, there is no significant trend in the MIZ extent in any of the observational datasets, with the exception of a small negative trend in Bootstrap in March of -0.52% or -0.520 x 10^{10} m^2 per year (Figure 1, Table 1). There

195 is also no significant trend in the modelled MIZ extent except for September (roughly 1.1% or -1.37x10^{10} km^2, $r^2 = 0.31$, Figure 1, Table 1). For most of the summer months, the spread of observations of MIZ extent is greater than the 10% error placed on each of the observations themselves (Figures 1b-d). This indicates that the observational error for the MIZ is larger than our assumed value of 10% based on Spreen et al. (2008). The modelled MIZ extent generally lies within the spread of the observations. The observations taken together provide lower and upper bounds for MIZ extent of between roughly 5-15 x10^5

200 km^2 for March, 15-50 x10^5 km^2 for July, 15-45 x10^5 km^2 for August, and 10-30 x10^5 km^2 for September (Figure 1).

The interannual variability of the MIZ (dashed lines in Figure 1) varies more than the sea ice extent in the observations as well as in the model results (Table 2). In the winter months (e.g. dashed lines in Figure 1a), the MIZ extent is more consistent across the datasets. In March, there are significant correlations between the MIZ extent observations (>0.889, Table 2) as well

205 as for the model results. From July through August, the differences in the absolute MIZ extent become very pronounced (dashed lines in Figures 1b-d). In July, the AMSR and Bootstrap are the most highly correlated (0.869), with lower or insignificant values between the other datasets. In September, the AMSR is well correlated with the other observations of MIZ extent (0.805 with OSI-450 and 0.852 with Bootstrap, Table 1).

4.2 Fraction of MIZ relative to total sea ice extent

210 The trends for the MIZ fraction, i.e. MIZ extent divided by the sea ice extent, for all of the observations are insignificant for March, but slightly positive for July, August, and September with the exception of AMSR, which is insignificant for July and September (Figure 2, Table 1). The trends per year for July are +0.3% for OSI-450 and +0.2% for Bootstrap. In August, there is an increase in MIZ fraction per year of 0.5% for OSI-450, 0.3% for Bootstrap, and 0.8% for AMSR. In September, the positive significant trends per year are 0.4% for OSI-450 and 0.3% for Bootstrap. The positive trend in MIZ fraction is given

215 by the stable MIZ extent and decline in sea ice extent (compare dashed and solid lines in Figure 1). The MIZ fraction for OSI-450 is consistently higher compared to the other observational datasets (Figure 2). The Bootstrap MIZ extent (absolute) is lower than OSI-450, which is the main reason for its lower MIZ fraction. The MIZ fraction for the model is insignificant for March, but slightly positive for July, August and September at +0.9%, +1.0% and 0.3% per year, respectively. In July, CICE-CPOM-2019 model shows a trend in MIZ fraction three times that of the OSI-450 and over four times that of the Bootstrap

220 dataset. In August, the model shows a trend two times that of OSI-450 and over three times that of Bootstrap. In September, the trends of MIZ fraction become roughly the same in the model and observations, and this remains so during the winter months (Table 1).

The modelled MIZ fraction generally lies within the spread of the observations with the exception of August, where it is
overestimated (Figure 2). The observations taken together provide lower and upper bounds for the MIZ fraction of roughly
0.050-0.10 for March, 0.17-0.52 for July, 0.21-0.57 for August, and 0.4-0.15 for September. The correlations between the
model and observations tend to be lower than the correlations between the observations themselves (Table 2). High
correlations (>0.843) exist between the Bootstrap and AMSR relative MIZ extent values for all months examined, with
generally lower values in July and August between Bootstrap and OSI-450.

4.3 MIZ trending northwards

There is no trend in the absolute MIZ extent (dashed lines in Figure 1), but the location of the MIZ in the more recent years is
further northwards, towards the pole. August 1993 (Figure 3a) and August 2013 (Figure 3b) illustrate that in 20 years the MIZ
has shifted northwards, and the ice pack has become separated by stretches of MIZ. The similar ice extent contours (15% sea
ice concentration, given by the solid lines in Figure 3) illustrate that the similar magnitude of ice extent (Figure 1) are also
consistent with ice location. The pack ice contours (dashed lines in Figure 3) show differences between the datasets, accounting
for the variability and differences in the MIZ extent (Figure 1, Table 2). In 1993, the pack ice is not separated by areas of
partial ice cover (Figure 3a) as it is in 2013 (Figure 3b). The MIZ is covers more of the central Arctic in the more recent year
(2013) than it does in 1993. Our results are robust given changes in the upper and lower bounds of the sea ice concentration
thresholds in the MIZ definition.

5 Discussion

5.1 Trends and correlations between observations and model

The lack of trend in the MIZ extent contrasts with the significant decline in total sea ice extent (Figure 1, Table 1). While
September is a common month to examine for projecting future sea ice extent since it is the month of the year where sea ice
reaches its annual minimum (Comiso et al., 2008), it is interesting to note that for studies of the MIZ, it is July and August
which may be more informative because these months show the greatest differences in trends of MIZ fraction between the
observational and model results (Table 1). These seasonal differences in observations of the MIZ fraction and model result
will have consequences for any future projections of the MIZ, and one must be wary of monthly extrapolation in particular
during the summer months.

The size of the MIZ is poorly defined by observations, and it follows that models of the MIZ can only be constrained within
these observational values. There have been recent developments in modelling of the MIZ, such as how waves break up the
ice (Meylan and Bennetts, 2018), the simulation of the floe size distribution and changes of sea ice floe size (Roach et al.,
2018), and how sea ice floe size information is important for accurately capturing the seasonality of sea ice concentration in

climate models (Bateson et al., 2019). However, the results in this study highlight the fact that attention must also be given to
255 improving observations of the MIZ location and extent in order to validate such models. It is important to note that while the
relative MIZ extent is slightly increasing, it does not necessarily follow that the MIZ extent itself is also increasing.

5.2 MIZ trending northward

Since the MIZ extent remains constant, it then follows that the central pack ice extent is decreasing because the total ice extent
is decreasing (Figure 1). Because the width of the MIZ is increasing in summer (Strong and Rigor, 2013) while the total extent
260 remains constant then the perimeter around the MIZ must be decreasing, forcing a northward movement (Figure 3). This is
consistent with the positive trend in the area-weighted latitude of the MIZ found for the same months with the same MIZ
definition in Strong and Rigor (2013). This northward migration of the MIZ has broad implications for changes in the coupled
bio-geo-physical climate system.

265 A declining sea ice cover in summer is a main contributor to the amplification of increasing temperatures in the Arctic (Screen
and Simmonds, 2010). The MIZ is also a potential area for Arctic cyclogenesis, which allows for significant heat release from
the ocean to the atmosphere (Inoue and Hori, 2011), thus contributing to the temperature amplification. With a northward
shifting storm track (Sepp and Jaagus, 2011), a northward shift of meridional heat transport is also expected. In addition,
changes in MIZ location will have regional implications for total momentum transfer from the atmosphere to the ocean through
270 the ice, because maximum momentum transfer occurs at moderate ice concentrations (~70-90%), full ice cover, and low ice
concentrations (~10-30%) (Cole et al., 2017; Tsamados et al., 2014) and is also impacted with varying surface roughness
(Martin et al., 2016).

From a biological perspective, it has already been established that sea ice receding further from the coastline followed by the
275 MIZ is a problem for marine mammals who use the sea ice as a platform for resting, hunting and breeding (Kovacs et al.,
2011). When there is no ice to rest on, there have been increasing accounts of animals changing their behaviour to use land as
a refuge. For example, walrus have been increasingly observed in mass haul-outs (Jay et al., 2012) resulting in premature
death due to overcrowding.

5.3 Sources of error

280 Observational uncertainty is one factor among others which must be considered when assessing the accuracy of any model
(Notz, 2015), including the CICE-CPOM-2019 model used here. An error of 10% applied to the observational products in
this study is consistent with other studies, as noted in Section 3.2. The error of 10% has been chosen because it is consistent
with the systematic differences between the ASI algorithm used to generate the AMSR data and other observational products
(NASA Team 2 and Bootstrap) are approximately 10% (Spreen et al., 2008). Comiso and Steffen, (2001) found an error range
285 between visible/infrared-derived ice concentrations (e.g. AVHRR) of 5-20%. The error between AVHRR products and other

SSM/I products ranging from 0.7 and 10.5% (with 5.3% error between AVHRR and Bootstrap) (Meier, 2005). A source of error for SSM/I concentrations is the use of hemispheric tie-points, which are unchanging and may not agree on conditions at a specific time and place (Meier, 2005). As well, since SSM/I concentrations are calculated based on daily composites of brightness temperatures and then averaged onto a 25-km resolution grid, it will result in errors stemming from spatial and 290 temporal averaging (Meier, 2005). Our study reveals that the systematic error in deriving the MIZ from these satellite products must be larger than 10% as documented by differences in monthly mean MIZ values of up to 300% (Figure 1).

6 Conclusions

We have analyzed the evolution of the absolute and relative marginal ice zone from 1979 through 2017 based on four satellite retrievals (OSI-450, Bootstrap, AMSR-E, and AMSR-2) and simulations with a stand-alone sea ice model CICE-CPOM-2019 295 including a floe size distribution model. While all products agree within their uncertainties during winter, big discrepancies occur during summer between the satellite products. We have found no significant trend in the MIZ extent across any of the observational datasets examined here (OSI-450, Bootstrap, and AMSR), with the exception of a small negative trend in March for Bootstrap. Due to the decrease in Arctic sea ice extent, there is a small positive trend for the relative MIZ extent at +0.2-0.3%/y in July, 0.3-0.8%/y in August, and 0.3-0.4%/y in September. During July and August, the positive trend is 2 to 4 times 300 stronger in our model simulation. Due to the spread of the observations in MIZ extent, we should be cautious about what conclusions we make about whether or not there is a true trend in the MIZ extent, and how well we can validate our MIZ models. Given this uncertainty, the fact that climate model projections show the Arctic becoming seasonally ice free by the mid-century (Notz and Stroeve, 2018) does not mean we will have an increased area of the ocean covered by marginal ice as defined by the 15-80% ice cover threshold definition. Only at the point when there is a completely seasonal ice cover in 305 conjunction with no pack ice, would our results suggest that further ice loss will result in decreases in MIZ extent.

Author contribution: RR performed the model simulations and wrote the code for analysis. RR wrote the manuscript with contributions from DF and DS.

310 *Acknowledgements:* This research was funded by the National Environment Research Council of the UK (NERC), Award number NE/R000654/1.

Competing interests: Daniel Feltham and David Schröder are members of the editorial board of the journal.

315 **References**

Aksenov, Y., Popova, E. E., Yool, A., Nurser, A. J. G., Williams, T. D., Bertino, L. and Bergh, J.: On the future navigability of Arctic sea routes: High-resolution projections of the Arctic Ocean and sea ice, Mar. Policy, doi:10.1016/j.marpol.2015.12.027, 2017.

Alexander, V. and Niebauer, H. J.: Oceanography of the eastern Bering Sea ice-edge zone in spring1, Limnol. Oceanogr.,
320 doi:10.4319/lo.1981.26.6.1111, 1981.

Amip-ii, N. D. O. E., R-, R., Kanamitsu, M., Ebisuzaki, W., Woollen, J., Yang, S.-K., Hnilo, J. J., Fiorino, M. and Potter, G. L.: NCEP–DOE AMIP-II Reanalysis (R-2), Bull. Am. Meteorol. Soc., doi:10.1175/BAMS-83-11-1631, 2002.

Barber, D. G., Hop, H., Mundy, C. J., Else, B., Dmitrenko, I. A., Tremblay, J. E., Ehn, J. K., Assmy, P., Daase, M., Candlish, L. M. and Rysgaard, S.: Selected physical, biological and biogeochemical implications of a rapidly changing Arctic Marginal
325 Ice Zone, Prog. Oceanogr., doi:10.1016/j.pocean.2015.09.003, 2015.

Bateson, A. W., Feltham, D. L., Schröder, D., Hosekova, L., Ridley, J. K. and Aksenov, Y.: Impact of floe size distribution on seasonal fragmentation and melt of Arctic sea ice, Cryosph. Discuss., 1–35, doi:10.5194/tc-2019-44, 2019.

Bennetts, L. G., O'Farrell, S. and Uotila, P.: Brief communication: Impacts of ocean-wave-induced breakup of Antarctic sea ice via thermodynamics in a stand-alone version of the CICE sea-ice model, Cryosphere, 11(3), 1035–1040, doi:10.5194/tc-
330 11-1035-2017, 2017.

Bitz, C. M. and Lipscomb, W. H.: An energy-conserving thermodynamic model of sea ice, J. Geophys. Res. Ocean., doi:10.1029/1999jc900100, 1999.

Boé, J., Hall, A. and Qu, X.: September sea-ice cover in the Arctic Ocean projected to vanish by 2100, Nat. Geosci., doi:10.1038/ngeo467, 2009.

335 Boutin, G., Lique, C., Ardhuin, F., Rousset, C., Talandier, C., Accensi, M. and Girard-Ardhuin, F.: Toward a coupled model to investigate wave-sea ice interactions in the Arctic marginal ice zone, Cryosph. Discuss., 1–39, doi:10.5194/tc-2019-92, 2019.

Briegleb, P. and Light, B.: A Delta-Eddington mutiple scattering parameterization for solar radiation in the sea ice component of the community climate system model, 2007.

340 Cole, S. T., Toole, J. M., Lele, R., Timmermans, M.-L., Gallaher, S. G., Stanton, T. P., Shaw, W. J., Hwang, B., Maksym, T., Wilkinson, J. P., Ortiz, M., Graber, H., Rainville, L., Petty, A. A., Farrell, S. L., Richter-Menge, J. A. and Haas, C.: Ice and ocean velocity in the Arctic marginal ice zone: Ice roughness and momentum transfer, , doi:10.1525/elementa.241, 2017.

Collins, C. O., Rogers, W. E., Marchenko, A. and Babanin, A. V.: In situ measurements of an energetic wave event in the Arctic marginal ice zone, Geophys. Res. Lett., 42(6), 1863–1870, doi:10.1002/2015GL063063, 2015.

345 Comiso, J.: Algorithm Theoretical Basis Document: AMSR-E Bootstrap Sea Ice Algorithm., 2012.

Comiso, J. C. and Steffen, K.: Studies of Antarctic sea ice concentrations from satellite data and their applications, J. Geophys. Res. Ocean., 106(C12), 31361–31385, doi:10.1029/2001jc000823, 2001.

Comiso, J. C., Parkinson, C. L., Gersten, R. and Stock, L.: Accelerated decline in the Arctic sea ice cover, Geophys. Res. Lett., 35(1), doi:10.1029/2007GL031972, 2008.

350 Dumont, D., Kohout, A. and Bertino, L.: A wave-based model for the marginal ice zone including a floe breaking parameterization, J. Geophys. Res. Ocean., 116(4), doi:10.1029/2010JC006682, 2011.

Ferry, N., Masina, S., Storto, A., Haines, K. and Valdivieso, M.: Product user manual global-reanalysis-phys-001-004-a and b, 2011.

Flocco, D., Feltham, D. L. and Turner, A. K.: Incorporation of a physically based melt pond scheme into the sea ice component

355 of a climate model, J. Geophys. Res. Ocean., doi:10.1029/2009JC005568, 2010.

Flocco, D., Schroeder, D., Feltham, D. L. and Hunke, E. C.: Impact of melt ponds on Arctic sea ice simulations from 1990 to 2007, J. Geophys. Res. Ocean., doi:10.1029/2012JC008195, 2012.

Hansen, B., Christiansen, S. and Pedersen, G.: Plankton dynamics in the marginal ice zone of the central Barents Sea during spring: Carbon flow and structure of the grazer food chain, Polar Biol., doi:10.1007/BF02390432, 1996.

360 Heorton, H. D. B. S., Feltham, D. L. and Tsamados, M.: Stress and deformation characteristics of sea ice in a high-resolution, anisotropic sea ice model, Philos. Trans. R. Soc. A Math. Phys. Eng. Sci., doi:10.1098/rsta.2017.0349, 2018.

Horvat, C. and Tziperman, E.: A prognostic model of the sea-ice floe size and thickness distribution, Cryosphere, 9(6), 2119–2134, doi:10.5194/tc-9-2119-2015, 2015.

Hunke, E. C., Lipscomb, W. H., Turner, A. K., Jeffery, N. and Elliott, S.: CICE: the Los Alamos Sea Ice Model Documentation

365 and Software User's Manual Version 5.1 LA-CC-06-012. [online] Available from: http://oceans11.lanl.gov/trac/CICE/wiki., 2015.

Inoue, J. and Hori, M. E.: Arctic cyclogenesis at the marginal ice zone: A contributory mechanism for the temperature amplification?, Geophys. Res. Lett., 38(12), doi:10.1029/2011GL047696, 2011.

IPCC, I. P. on C. C.: Climate Change 2014: Synthesis Report. Contribution of Working Groups I, II and III., Geneva, Switz.

370 IPCC, 151, 2014.

Jay, C. V., Fischbach, A. S. and Kochnev, A. A.: Walrus areas of use in the Chukchi Sea during sparse sea ice cover, Mar. Ecol. Prog. Ser., doi:10.3354/meps10057, 2012.

Kovacs, K. M., Lydersen, C., Overland, J. E. and Moore, S. E.: Impacts of changing sea-ice conditions on Arctic marine mammals, Mar. Biodivers., doi:10.1007/s12526-010-0061-0, 2011.

375 Kwok, R.: Arctic sea ice thickness, volume, and multiyear ice coverage: Losses and coupled variability (1958-2018), Environ. Res. Lett., 13(10), doi:10.1088/1748-9326/aae3ec, 2018.

Lavergne, T., Tonboe, R., Lavelle, J. and Eastwood, S.: EUMETSAT Ocean and Sea Ice SAF High Latitude Processing Centre Algorithm Theoretical Basis Document for the OSI SAF Global Sea Ice Concentration Climate Data Record Algorithm., 2016.

Lee, C. and Thomson, J.: An Autonomous Approach to Observing the Seasonal Ice Zone in the Western Arctic, Oceanography,

380 30(2), 56–68, doi:10.5670/oceanog.2017.222, 2017.

Lipscomb, W. H. and Hunke, E. C.: Modeling Sea Ice Transport Using Incremental Remapping, Mon. Weather Rev.,

doi:10.1175/1520-0493(2004)132<1341:msitui>2.0.co;2, 2004.

Madec, G. and Imbard, M.: A global ocean mesh to overcome the North Pole singularity, Clim. Dyn., 12(6), 381–388, doi:10.1007/BF00211684, 1996.

385 Martin, T., Tsamados, M., Schroeder, D. and Feltham, D. L.: The impact of variable sea ice roughness on changes in Arctic Ocean surface stress: A model study, J. Geophys. Res. Ocean., 121(3), 1931–1952, doi:10.1002/2015JC011186, 2016.

Maykut, G. A. and Untersteiner, N.: Some results from a time-dependent thermodynamic model of sea ice, J. Geophys. Res., doi:10.1029/jc076i006p01550, 1971.

Meier, W. N.: Comparison of passive microwave ice concentration algorithm retrievals with AVHRR imagery in arctic
390 peripheral seas, IEEE Trans. Geosci. Remote Sens., 43(6), 1324–1337, doi:10.1109/TGRS.2005.846151, 2005.

Meylan, M. H. and Bennetts, L. G.: Three-dimensional time-domain scattering of waves in the marginal ice zone, Philos. Trans. R. Soc. A Math. Phys. Eng. Sci., doi:10.1098/rsta.2017.0334, 2018.

Notz, D.: How well must climate models agree with observations?, Philos. Trans. R. Soc. A Math. Phys. Eng. Sci., 373(2052), doi:10.1098/rsta.2014.0164, 2015.

395 Notz, D. and Stroeve, J.: The Trajectory Towards a Seasonally Ice-Free Arctic Ocean, Curr. Clim. Chang. Reports, doi:10.1007/s40641-018-0113-2, 2018.

Onarheim, I. H., Eldevik, T., Smedsrud, L. H. and Stroeve, J. C.: Seasonal and regional manifestation of Arctic sea ice loss, J. Clim., 31(12), 4917–4932, doi:10.1175/JCLI-D-17-0427.1, 2018.

Overland, J. E. and Wang, M.: Future regional Arctic sea ice declines, Geophys. Res. Lett., 34(17), L17705,
400 doi:10.1029/2007GL030808, 2007.

Petty, A. A., Holland, P. R. and Feltham, D. L.: Sea ice and the ocean mixed layer over the Antarctic shelf seas, Cryosphere, doi:10.5194/tc-8-761-2014, 2014.

Roach, L. A., Horvat, C., Dean, S. M. and Bitz, C. M.: An Emergent Sea Ice Floe Size Distribution in a Global Coupled Ocean-Sea Ice Model, J. Geophys. Res. Ocean., doi:10.1029/2017JC013692, 2018.

405 Rothrock, D. A.: The energetics of the plastic deformation of pack ice by ridging, J. Geophys. Res., doi:10.1029/jc080i033p04514, 1975.

Schröder, D., Feltham, D. L., Flocco, D. and Tsamados, M.: September Arctic sea-ice minimum predicted by spring melt-pond fraction, Nat. Clim. Chang., 4(5), 353–357, doi:10.1038/nclimate2203, 2014.

Schröder, D., Feltham, D. L., Tsamados, M., Ridout, A. and Tilling, R.: New insight from CryoSat-2 sea ice thickness for sea
410 ice modelling, , 125–139, 2019.

Screen, J. A. and Simmonds, I.: The central role of diminishing sea ice in recent Arctic temperature amplification, Nature, 464(7293), 1334–1337, doi:10.1038/nature09051, 2010.

Sepp, M. and Jaagus, J.: Changes in the activity and tracks of Arctic cyclones, Clim. Change, 105, 577–595, doi:10.1007/s10584-010-9893-7, 2011.

415 Serreze, M. C., Holland, M. M. and Stroeve, J.: Perspectives on the Arctic's shrinking sea-ice cover, Science (80-.).,

315(5818), 1533–1536 [online] Available from: http://www.sciencemag.org/content/315/5818/1533.short (Accessed 22 October 2014), 2007.

Spreen, G., Kaleschke, L. and Heygster, G.: Sea ice remote sensing using AMSR-E 89-GHz channels, J. Geophys. Res. Ocean., 113(2), doi:10.1029/2005JC003384, 2008.

420 Stroeve, J., Holland, M. M., Meier, W., Scambos, T. and Serreze, M.: Arctic sea ice decline: Faster than forecast, Geophys. Res. Lett., 34(9), doi:10.1029/2007GL029703@10.1002/(ISSN)1944-8007.GRL40, 2007.

Strong, C. and Rigor, I. G.: Arctic marginal ice zone trending wider in summer and narrower in winter, Geophys. Res. Lett., 40(18), 4864–4868, doi:10.1002/grl.50928, 2013.

Strong, C., Foster, D., Cherkaev, E., Eisenman, I. and Golden, K. M.: On the definition of marginal ice zone width, J. Atmos.
425 Ocean. Technol., 34(7), 1565–1584, doi:10.1175/JTECH-D-16-0171.1, 2017.

Svendsen, E.: Norwegian Remote Sensing Experiment: evaluation of the Nimbus 7 scanning multichannel microwave radiometer for sea ice research., J. Geophys. Res., 88(C5), 2781–2791, doi:10.1029/JC088iC05p02781, 1983.

Svendsen, E., Matzler, C. and Grenfell, T. C.: A model for retrieving total sea ice concentration from a spaceborne dual-polarized passive microwave instrument operating near 90 ghz, Int. J. Remote Sens., 8(10), 1479–1487,
430 doi:10.1080/01431168708954790, 1987.

Thomson, J. and Rogers, W. E.: Swell and sea in the emerging Arctic Ocean, Geophys. Res. Lett., 41(9), 3136–3140, doi:10.1002/2014GL059983, 2014.

Thorndike, A. S., Rothrock, D. A., Maykut, G. A. and Colony, R.: The thickness distribution of sea ice, J. Geophys. Res., 80(33), 4501–4513, doi:10.1029/jc080i033p04501, 1975.

435 Tsamados, M., Feltham, D. L., Schroeder, D., Flocco, D., Farrell, S. L., Kurtz, N., Laxon, S. W. and Bacon, S.: Impact of Variable Atmospheric and Oceanic Form Drag on Simulations of Arctic Sea Ice*, J. Phys. Oceanogr., doi:10.1175/jpo-d-13-0215.1, 2014.

Tsamados, M., Feltham, D., Petty, A., Schroeder, D. and Flocco, D.: Processes controlling surface, bottom and lateral melt of Arctic sea ice in a state of the art sea icemodel, Philos. Trans. R. Soc. A Math. Phys. Eng. Sci., 373(2052),
440 doi:10.1098/rsta.2014.0167, 2015.

Wilchinsky, A. V. and Feltham, D. L.: Modelling the rheology of sea ice as a collection of diamond-shaped floes, J. Nonnewton. Fluid Mech., doi:10.1016/j.jnnfm.2006.05.001, 2006.

Zhang, J., Stern, H., Hwang, B., Schweiger, A., Steele, M., Stark, M. and Graber, H. C.: Modeling the seasonal evolution of the Arctic sea ice floe size distribution, Elementa, 4, doi:10.12952/journal.elementa.000126, 2016.

445
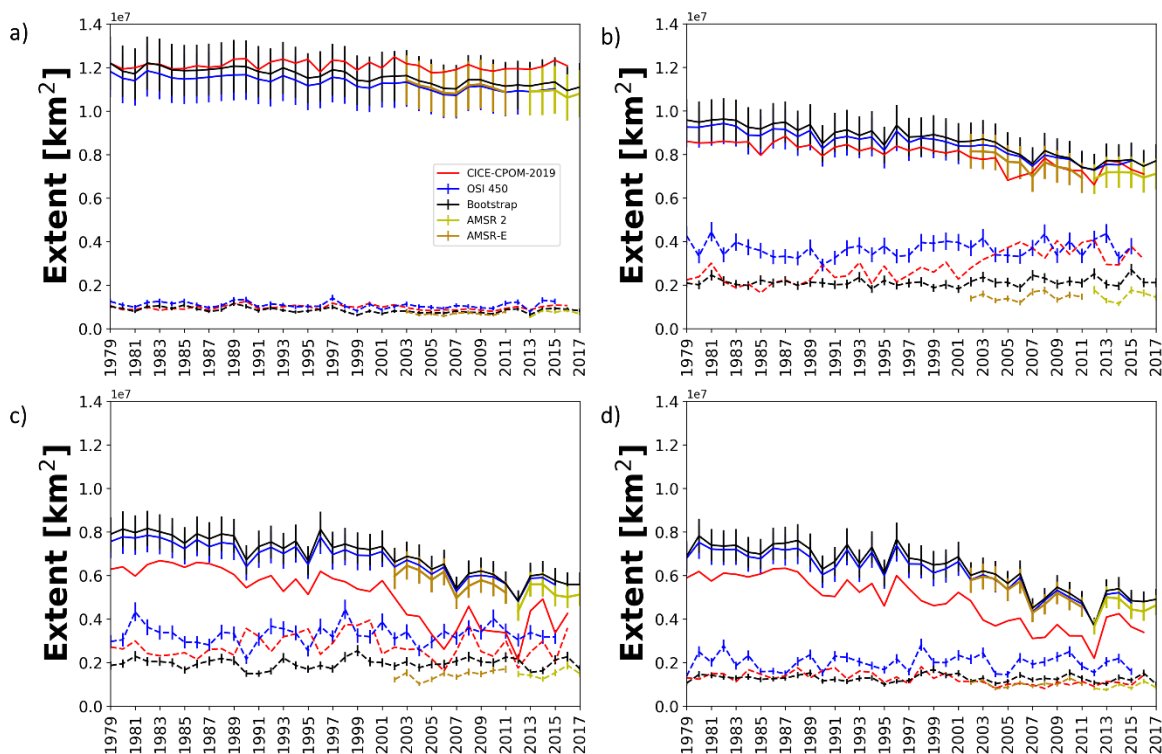
Figure 1: Arctic sea ice extent (solid lines) and marginal ice zone extent (dashed lines) from our CICE simulation CICE-CPOM-2019 and four remote sensing products for (a) March (b) July (c) August (d) September. Marginal ice zone extent is defined at the area where sea ice concentration is between 15-80%. Sea ice extent is the area of ice coverage above 15%. An error bar of 10% has been applied to the observational output.
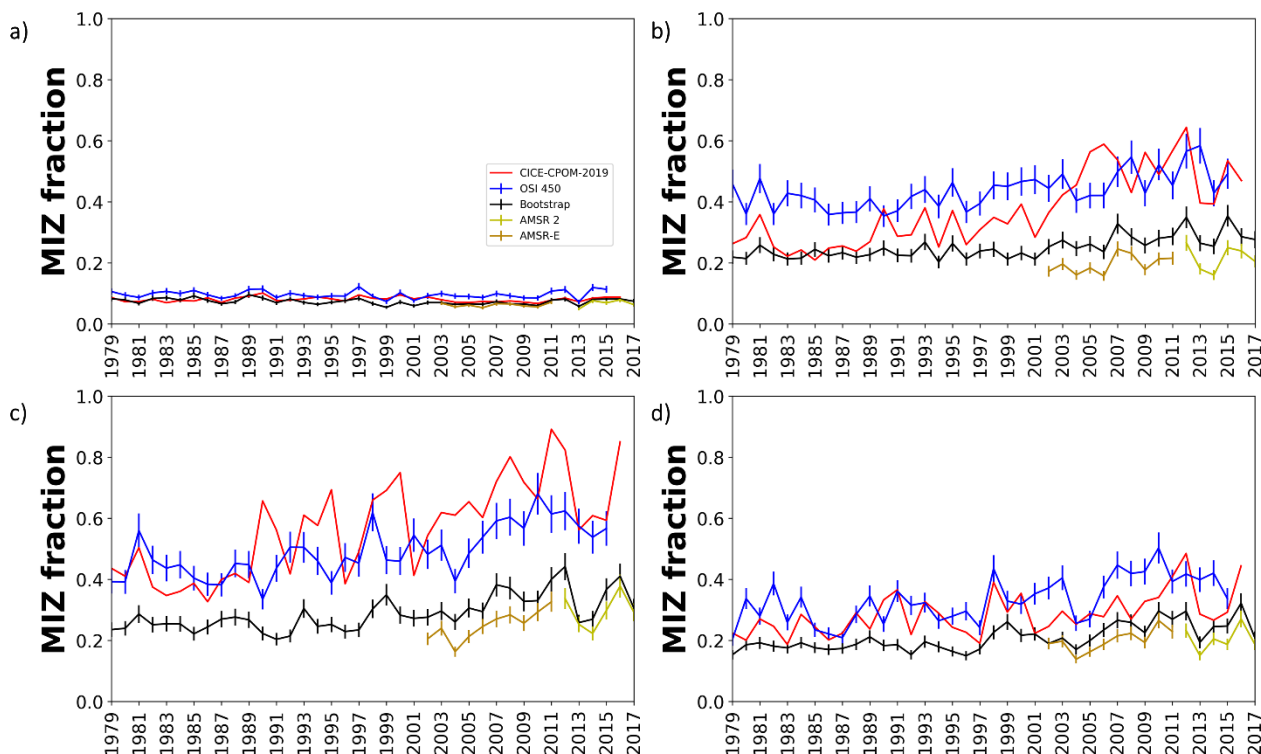
Figure 2: As Figure 1, but MIZ fraction for (a) March (b) July (c) August (d) September. Marginal ice zone extent is defined at the
area where sea ice concentration is between 15-80%. Sea ice extent is the area of ice coverage above 15%. An error bar of 10% has
been applied to the observational output.
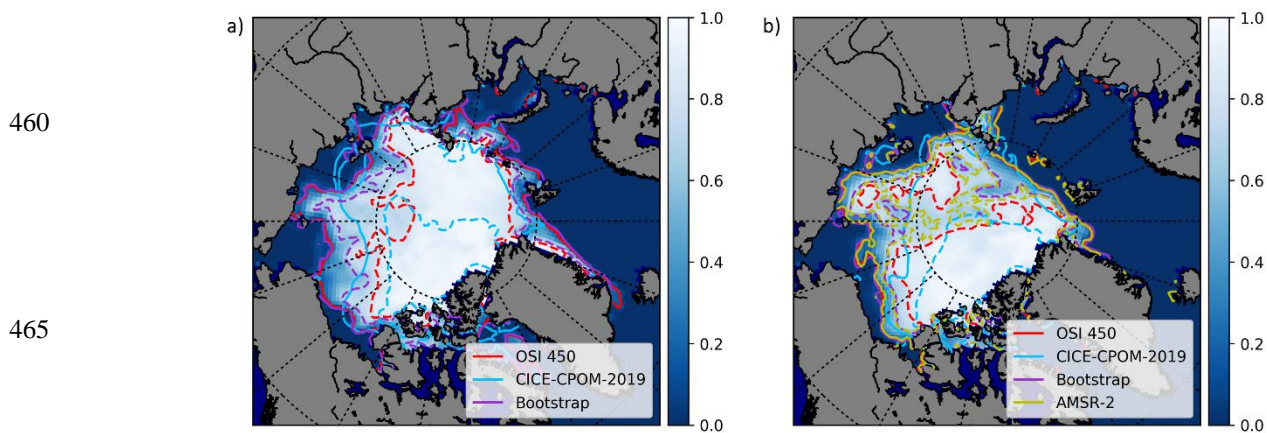
Figure 3: The location of the MIZ for August 1993 (a) and August 2013 (b). The MIZ seems to be trending northwards in recent
years. Dashed and solid lines represent the 80% and 15% sea ice concentration levels, respectively. AMSR data is not available prior
to 2002. Underlying sea ice concentration is from the OSI-450 satellite product.

$\alpha = 0.05$

Trend in 10^{10} m^2 per year (r^2)			Relative MIZ
March	**Total ice extent**	**MIZ extent**	**(MIZ extent/total ice extent) [1/year]**
OSI 450	-2.42 (0.74)	Insig.	Insig.
Bootstrap	-2.76 (0.78)	-0.520	Insig.
AMSR	-3.04 (0.43)*	Insig.*	Insig.*
CICE-CPOM-2019	Insig.	Insig.	Insig.
July			
OSI 450	-5.27 (0.84)	Insig.	+0.003 (0.375)
Bootstrap	-5.85 (0.87)	Insig.	+0.002 (0.450)
AMSR	-7.55 (0.67)*	Insig.*	Insig.*
CICE-CPOM-2019	-4.29 (0.70)	Insig.	+0.009 (0.636)
August			
OSI 450	-6.52 (0.78)	Insig.	+0.005 (0.479)
Bootstrap	-7.19 (0.81)	Insig.	+0.003 (0.444)
AMSR	-7.96 (0.47)*	Insig.*	+0.008 (0.672)*
CICE-CPOM-2019	-9.61 (0.71)	Insig.	+0.010 (0.557)
September			
OSI 450	-7.80 (0.75)	Insig.	+0.004 (0.392)
Bootstrap	-8.07 (0.75)	Insig.	+0.003 (0.479)
AMSR	-9.72 (0.50)*	Insig.*	Insig.*
CICE-CPOM-2019	-9.02 (0.79)	-1.37 (0.31)	+0.003 (0.293)

Table 1: Trends with r^2 values in brackets for total sea ice extent, MIZ extent, and extent of the MIZ relative to the total sea ice extent for the model run and all observational datasets examined. Note that the periods between above datasets are not the same: OSI-450 (1979-2015), CICE-CPOM-2019 (1979-2017), Bootstrap (1979-2017), and AMSR (June 2002 – 4 Oct 2011 AMSR-E, July 2012 – 2017 AMSR2). The AMSR trends are denoted with * to clearly indicate the shortened time coverage of those observations in comparison with the rest. The r^2 values are calculated using a linear least-squares regression and alpha represents a 95% confidence level.

α = 0.05

Correlations	Total ice extent			MIZ extent			Relative MIZ extent		
March	OSI 450	CICE19	Bootstrap	OSI 450	CICE19	Bootstrap	OSI 450	CICE19	Bootstrap
CICE-CPOM-2019	0.448			0.548			0.502		
Bootstrap	0.998	0.440		0.894	0.415		0.876	0.392	
AMSR*	0.957	Insig.	0.962	0.922	0.759	0.889	0.932	0.792	0.902
July	OSI 450	CICE19	Bootstrap	OSI 450	CICE19	Bootstrap	OSI 450	CICE19	Bootstrap
CICE-CPOM-2019	0.896			Insig.			0.547		
Bootstrap	0.996	0.913		0.362	0.414		0.655	0.778	
AMSR*	0.989	0.575	0.990	0.595	Insig.	0.869	0.645	Insig.	0.922
August	OSI 450	CICE19	Bootstrap	OSI 450	CICE19	Bootstrap	OSI 450	CICE19	Bootstrap
CICE-CPOM-2019	0.902			Insig.			0.539		
Bootstrap	0.998	0.900		0.472	Insig.		0.719	0.749	
AMSR*	0.991	Insig.	0.987	0.826	Insig.	0.637	0.886	0.755	0.843
September	OSI 450	CICE19	Bootstrap	OSI 450	CICE19	Bootstrap	OSI 450	CICE19	Bootstrap
CICE-CPOM-2019	0.957			Insig.			0.552		
Bootstrap	0.998	0.955		0.577	Insig.		0.755	0.719	
AMSR*	0.990	0.778	0.989	0.805	Insig.	0.852	0.780	0.675	0.927

Table 2: Correlations of the inter-annual variability for the total sea ice extent, MIZ extent, and extent of the MIZ relative to the total sea ice extent for the model run and all observational datasets examined. The AMSR trends are denoted with * to clearly indicate the shortened time coverage of those observations in comparison with the rest.